

Accepted Manuscript

Using post-flood surveys and geomorphologic mapping to evaluate hydrological and hydraulic models: the flash flood of the Girona River (Spain) in 2007

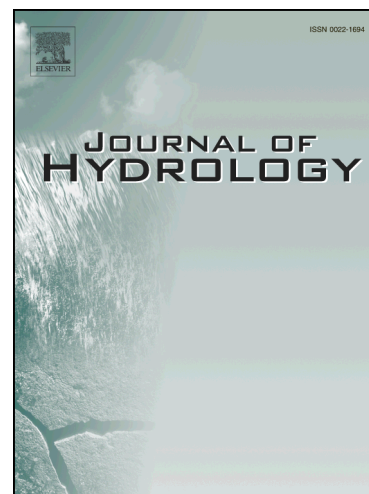
F. Segura-Beltrán, C. Sanchis-Ibor, M. Morales-Hernández, M. González-Sanchis, G. Bussi, E. Ortiz

PII: S0022-1694(16)30230-X

DOI: <http://dx.doi.org/10.1016/j.jhydrol.2016.04.039>

Reference: HYDROL 21209

To appear in: *Journal of Hydrology*



Please cite this article as: Segura-Beltrán, F., Sanchis-Ibor, C., Morales-Hernández, M., González-Sanchis, M., Bussi, G., Ortiz, E., Using post-flood surveys and geomorphologic mapping to evaluate hydrological and hydraulic models: the flash flood of the Girona River (Spain) in 2007, *Journal of Hydrology* (2016), doi: <http://dx.doi.org/10.1016/j.jhydrol.2016.04.039>

This is a PDF file of an unedited manuscript that has been accepted for publication. As a service to our customers we are providing this early version of the manuscript. The manuscript will undergo copyediting, typesetting, and review of the resulting proof before it is published in its final form. Please note that during the production process errors may be discovered which could affect the content, and all legal disclaimers that apply to the journal pertain.

Using post-flood surveys and geomorphologic mapping to
evaluate hydrological and hydraulic models: the flash flood of the
Girona River (Spain) in 2007

Segura-Beltrán, F.¹; Sanchis-Ibor, C.²; Morales-Hernández, M.³; González-Sanchis,
M.⁴; Bussi, G.⁵ and Ortiz, E.⁶.

¹ Departament de Geografia, Universitat de València, Avda./Blasco Ibáñez 28, 46010, València, Spain

² Centro Valenciano de Estudios del Riego, Universitat Politècnica de València, 46022, València, Spain

³ Fluid Mechanics, LIFTEC-EINA, CSIC-Universidad Zaragoza, C/ María de Luna 3, 50018, Zaragoza,
Spain

⁴ Department of Hydraulic Engineering and Environment, Universitat Politècnica de València, València,
Spain

⁵ School of Geography and the Environment, University of Oxford, South Parks Road, OX1 3QY,
Oxford, UK

⁶ Idrologia & Ambiente s.r.l. Via Stazio 66 80123 Napoli, Italy

Abstract

This paper analyses the Girona River (Spain) flash flood, occurred on the 12th of
October 2007, combining hydrological and hydraulic modeling with geomorphologic
mapping and post-flood survey information. This research aims to reproduce the flood
event in order to understand and decipher the flood processes and dynamics on a system

of overlapped prograding alluvial fans. The hydrological model TETIS was used to characterize the shape and dimension of the October 2007 Girona River hydrograph. Subsequently, the flood event was reproduced using the free surface flow module of the model RiverFlow2D. The combination of hydrological and hydraulic models was evaluated using post-flood surveys defining maximum flooded area and flood depths. Then, simulations with different peak discharges were carried out to estimate the hydro-geomorphologic response of the Girona River floodplain, through the identification of the activation thresholds in different geomorphic elements.

Results showed that the unit peak discharge of the October 2007 flood event ($5 \text{ m}^3 \text{ s}^{-1} \text{ km}^{-2}$) was among the largest ever recorded in the area, according to the existing literature. Likewise, the hydraulic model showed a good performance in reproducing the flood event ($\text{Fit}_A = 76 \%$, $\text{RMSE} = 0.65 \text{ m}$ and $\text{NSE} = 0.6$), despite the complexity of the case, an ephemeral and ungauged river. The model simulation revealed the existence of an activation pattern of paleochannels and alluvial fans, which was altered by the presence of some anthropogenic disturbances.

This multidisciplinary approach proved to be a useful strategy for understanding flash flood processes in ungauged catchments. It allowed understanding the mechanisms governing floods in alluvial fans systems and it represented a solid contribution for early warning plans and risk mitigation policies.

Keywords: Flash floods; hydrological modeling; hydraulic modeling; alluvial fans; post-flood surveys; geomorphologic mapping; Mediterranean Spain.

52

53 1. Introduction

54

55 Flash floods are a recurrent cause of damages and fatalities. According to Barredo
56 (2007), 40% of the flood-related casualties that occurred in Europe in the period 1950–
57 2006 are due to this type of flood events, which take place in different geographical
58 scenarios (Gaume et al., 2009; Marchi et al., 2010; Borga and Morin, 2014; Llasat et al.,
59 2014). However, they are particularly frequent and relevant in ungauged ephemeral
60 streams in arid and semiarid zones (House and Baker, 2001; Yatheendradas et al.,
61 2008). These events are a consequence of intense rainfall and sudden runoff generation.
62 The flash flood hydrographs have steep rising limbs, sharp peaks and large transmission
63 losses (Nanson et al., 2002). The runoff coefficient has a high variability (Camarasa-
64 Belmonte and Segura-Beltrán, 2001; Braud et. al., 2010) depending on basin lithology,
65 soil characteristics and antecedent soil moisture.

66

67 In the Western Mediterranean region, flash floods usually occur in spring and autumn,
68 when intense, heavy and irregularly distributed rain takes place (Segura-Beltrán, 1990;
69 Camarasa-Belmonte and Segura-Beltrán, 2001; Barredo, 2007; Gaume et al. 2009). The
70 particular conformation of the Mediterranean basin, with high mountain ranges close to
71 the sea, steep slopes, sparse vegetation, thin soils and permeable rock, enhances the
72 magnitude of these natural events. Alluvial fan coastal systems, such as the Girona
73 River floodplain (eastern Spain), introduce a major complexity on flooding processes
74 and risk management (Segura-Beltrán, 2003; Santangelo et al., 2012), because of the
75 uncertainty derived from convex topography, channel mobility and overlapping
76 sequences.

77

78 The impact of flash floods in this region is increased by the intense human use of the
79 narrow Mediterranean coastal plains. These areas, densely populated, concentrate the
80 most part of the urban developments, infrastructures and economic activity of the
81 region. The absence of sound territorial planning in these vulnerable areas usually
82 worsens the consequences of flash floods (Barrera et al., 2006; Lara et al., 2010;
83 Camarasa-Belmonte and Soriano-García, 2012). For these reasons, improving the
84 knowledge on these phenomena is a critical factor in developing resilient adaptation
85 strategies (Creutin et al., 2013).

86

87 Despite the fact that there are numerous studies on flash floods, event comprehension
88 and flood risk management are not easy tasks. In the last decade, numerous hydrological
89 (Pilgrim et al., 1988; Vélez and Francés, 2005; Braud et al. 2010) and hydraulic models
90 (Hall et al., 2005; Bates et al., 2006; Pappenberger et al., 2005 and 2007; Schuman et al.
91 2009; Di Baldassarre et al. 2009; Murillo and García-Navarro, 2010; Lacasta et al.,
92 2014) have been developed to simulate flood hydrographs and flooded areas. However,
93 the specific space-time scales of flash flood events, the lack or scarcity of rainfall and
94 streamflow data, and the short lag time are a cause of high uncertainty. In order to
95 overcome these difficulties, flash flood modeling requires an integrated approach that
96 includes, besides the hydrological and hydraulic models, information such as hydro-
97 geomorphic mapping and post-flood surveys (Borga, et al. 2011; Gaume and Borga,
98 2008; Marchi et al. 2010) so as to incorporate qualitative information to achieve a better
99 understanding of flood processes.

100

101 This study analyses the Girona River flash flood, which occurred on the 12th of October
102 2007. This event caused one casualty and material damages to 1,000 buildings, 1,500
103 vehicles and numerous agricultural and road infrastructures. Rainfall parameters were
104 exceptional, in terms of intensity and accumulated precipitation. In some locations,
105 more than 400 mm accumulated rainfall was registered in 48 hours. The fact that this
106 flash-flood has been well documented (Segura-Beltrán, 2009; Pastor et al., 2010) and
107 the development of geomorphologic works bring us some new approaches in order to
108 test hydrological and hydraulic models, considering post-flood surveys and hydro-
109 geomorphic mapping in order to validate the hydrologic and hydraulic models used to
110 simulate the event.

111

112 Our study has four major objectives: i) to implement a hydrological and a hydraulic
113 model in order to reproduce the October 2007 flash flood, ii) to evaluate the model
114 performances in reproducing the aforementioned flood event through the comparison
115 between model results and post-flood survey levels information, iii) to understand and
116 decipher the flooding processes in alluvial fans systems combining the use of
117 geomorphologic mapping and hydraulic simulations, and in addition, iv) to provide
118 information to improve flood risk management.

119

120

121 2. Study site

122

123 2.1. The Girona River basin

124

125 The Girona River basin is located in the Eastern part of the Iberian Peninsula, within the
 126 administrative territory of the Province of Alicante (Spain). The river flows through the
 127 Baetic Cordillera from west to east, along 32 km. The basin area at the river mouth into
 128 the Mediterranean Sea is 117.7 km². The catchment encompasses various calcareous
 129 mountains with a SW-NE orientation, separated by several corridors covered by
 130 Miocene marls (Figure 1). The river is semi-ephemeral, and presents high transmission
 131 losses, combining dry, intermittent and wet reaches.

132

133 The Girona River sources are located at 1,300 m above the sea level. The river crosses
 134 the Ebo Valley, a graben filled with tertiary marls, and downstream it flows through the
 135 Laguar Valley, a deep calcareous canyon cut across Secondary deposits. This canyon
 136 was used in 1945 to construct the Isbert Reservoir (capacity 1 Mm³), now partially
 137 silted and abandoned. Downstream, at the Rectoria Valley, the river built a large
 138 floodplain. The river flows into the Mediterranean at the Almadrava Cape.

139

140 The climate in the area is Mediterranean. Mean annual rainfall is between 600 and 900
 141 mm, with a maximum in autumn and a secondary peak in spring. Rainfall intensity in
 142 this area is the highest of the Iberian Peninsula (Martin-Vide, 2004) and the maximum
 143 accumulated rainfall in 24 hours is close to 1,000 mm at some observatories
 144 neighbouring the Girona River (Armengot, 1994). Consequently, flash floods are
 145 frequent, particularly in October.

146

147

148 2.2. The floodplain

149

150 The Girona floodplain is made of a complex sequence of Quaternary prograding and
151 coalescent alluvial deposits. Early Pleistocene sediments are present at the inner part of
152 the floodplain (Lendínez et al, 2008), at the Rectoria Valley. This valley is flanked by
153 the Segària and Segili mountains, and several small torrential fans (Figure 2). The
154 mountains constrain the alluvial fan expansion, creating a bajada of 5°-6° slope. The
155 Girona River dissects this bajada through a train of meanders, incised in late Quaternary
156 terraces. Two parallel tributaries (Bolata and Trullencs) drain the lateral inter-fan
157 depression (Figure 2).

158

159 Downstream Beniarbeig, the coastal plain widens. The Girona River has created a large
160 alluvial fan coalescent with the Alberca Ravine sediments, which Vegas et al. (1975)
161 attribute to Middle Pleistocene. To the west, the alluvial fan is flanked by the Segària
162 Mountains, formed by highly karstified Secondary limestone. To the south, various
163 Tertiary marly hills (Els Tossals, Torrecarrals) close the river floodplain. A Late
164 Pleistocene alluvial fan (Vegas et al., 1975) overlaps the Middle Pleistocene materials
165 upstream El Verger. This is an active fan, which has several lobes between El Verger
166 and the Mediterranean Sea. Finally, at the river mouth, there is a small Holocene fan
167 that forms a protuberance in the coastline (Almadrava Cape) (Fig. 2).

168

169 This system of overlapped and prograding alluvial fans, characteristic of the Valencian
170 coastal area, exhibits a complex surface morphology of multiple-age segments.

171 The internal stratigraphy of these systems reveals an 'ageing' sequence characterized by
172 a 'regime change' from aggradation to dissection. Periods of aggradation appear to have
173 coincided with Pleistocene global glacial phases and dissection phases relate to
174 interglacials (Segura-Beltrán, 1990; Segura-Beltrán, 2003 and Harvey, 2012). However,

the Holocene deposits appear to be unusual. Although most fan proximal areas are dominantly dissectional, many distal zones prograde, probably due to human-induced erosion (Harvey, 2002). This complex Quaternary sequence originates a prograding style. Prolonged fanhead incision causes downstream migration of the intersection points, as the fan morphology becomes progressively ‘telescopic’ (Harvey, 2012). The morphology of these fan systems has a determinant influence on flood hazard assessment. On prograding alluvial fans, flow usually exceeds the capacity of the stream channel at the apexes and intersection points, paleochannels drain fan surface, and inter-fan depressions and marshes accumulate overbank flow (Segura-Beltrán, 2003).

184

2.3. The October 2007 flood

186

The synoptic frame of the meteorological situation leading to the torrential rains of 11–12 October 2007 in the Valencia region was characterized by two phenomena: i) an easterly maritime wind advection across the Western Mediterranean, lasting for at least 48 hours, and ii) the presence of an upper-level isolated low over the Eastern Iberian Peninsula. The arrival of a moist air mass over the Valencia Region, and the presence of a cold pool aloft, caused torrential rainfall. The event was extensively described at the regional scale by Pastor et al. (2010).

194

The intense rainfall generated a flash flood, which affected the villages of Beniarbeig, El Verger and Els Poblets, and also the coastal urban area (Figure 1). At Beniarbeig, the CV-732 Bridge was destroyed. At El Verger, the flood was 2.4 m depth in some houses located on the river bank, and the river flow demolished a house and killed a woman. Most of the urban area of Els Poblets was also affected by the overbank flow.

200

201 According to Segura-Beltrán (2009), who analysed 12 observatories (Figure 3)
 202 belonging to the Automatic Hydrological Information System (AHIS) of the Jucar Basin
 203 Authority (JBA), rainfall varied between 250 and 420 mm. The highest intensities (>
 204 150 mm/h) were recorded between 10:00 and 12:00 AM (12th October), particularly in
 205 the middle and upper basin areas (Figures 4a and 4b). Considering a mean catchment
 206 rainfall value of 343 mm, total rainfall was 35.2 Mm³. Rainfall progressively increased
 207 from the coastline to the inland areas. The highest rainfall values were recorded within
 208 the mountain areas (420 mm), whereas in the coastal plain precipitation was between
 209 250 and 300 mm.

210

211 The flood was generated in the headwaters area, and progressed towards the coastal
 212 area, supplied by the upper and middle basin tributaries. However, the low basin
 213 tributaries, such as Segària Mountain Range ravines, did not have relevant flow
 214 (Segura-Beltrán, 2009).

215

216

217 3. Materials and methods

218

219 This study combined hydrological and hydraulic modeling with geomorphology and
 220 post-flood survey in order to reproduce a particular flooding event and understand and
 221 decipher the flooding processes using geomorphologic mapping. First, the hydrological
 222 model TETIS (Francés et al., 2007) was used to estimate a range of possible
 223 hydrographs for the flood event of October 2007. Then, the range of hydrographs was
 224 simulated using free surface flow module of the model RiverFlow2D (Murillo and

García-Navarro, 2010; Lacasta et al., 2014). The results were then evaluated using geomorphology and post-flood survey information to select the hydrograph that shows the best agreement between simulated and observed information. Finally, this combination of hydrological and hydraulic modeling and geomorphology was used to provide information to improve flood risk management.

3.1. Hydrological modeling

The flash flood of October 2007 was reconstructed by means of the hydrological model TETIS (Francés et al., 2007), a distributed conceptual hydrological model widely used in Spain and other countries (e.g. Francés et al., 2011; Bussi et al., 2012; Vélez et al., 2009; Buendia et al. 2015; Rodríguez-Lloveras et al. 2015). In this model, the main components of the hydrological cycle are represented by means of tanks. The TETIS model has a specific split-structure of the parameters (Francés et al., 2007) which allows its calibration without altering the spatial structure of the parameter maps. The model calibration can be carried out by adjusting up to nine correction factors, which multiply each a corresponding parameter map.

The Digital Elevation Model (5x5 m resolution) was downloaded from the Spanish National Cartographic Centre (www.cnig.es). Nevertheless, the scale of soil (1: 50,000) and geological (1:50,000) maps, and land use maps resolution (1:100,000) was larger. Therefore, the modelers' expertise and previous modeling work with the TETIS model led to increase the mesh size and resample the digital elevation model to 100 x100 m as a compromise between model accuracy, resolution of the available information and computational time. The land-use map was obtained from the Corine Land Cover 2006

dataset, from the European Environment Agency (2007), while soil characteristic information was retrieved from local soil surveys and soil profiles. Geological maps were also used, obtained from the 1:50,000 geological series of the Spanish Geological Institute (IGME, www.igme.es). The soil retention capacity was computed as the difference between the soil water content at saturation and at the wilting point. These soil properties, as well as the soil infiltration capacity, were calculated depending on soil texture, organic content, soil structure and salinity according to Saxton and Rawls (2006) pedotransfer functions. The deep soil percolation capacity was estimated based on literature values for the geological formations found in this catchment, depending on their lithology, degree of fracturing and macroporosity.

The rainfall of seven rain gauges within and surrounding the Girona River catchment (Gallinera, Isbert, la Carrasca, Alcalalí, Guadalest, Algar and Assut de Mandem), with 5-minutes series, managed by the Júcar River Basin Authority (Confederación Hidrográfica del Júcar, CHJ) was used (Figure 3). The rainfall aggregation and interpolation was shown to be highly relevant in flash flood response and modeling (Borga et al., 2007; Anquetin et al., 2010; Nikolopoulos et al. 2011). In this study, the rain gauge station records were interpolated with a kriging technique, on a 1x1 km mesh and with a temporal resolution of 10 minutes. The spatial variations of the temperature were taken into account by assigning a value to each cell of the 100 x100 m mesh depending on their distance from the meteorological stations, employing the Thiessen polygons methodology. No reliable water discharge records were available for the Girona River catchment. For this reason, a nearby similar catchment was used to implement the model: the Guadalest reservoir (54.34 km² drainage basin area) (Figure 3). The TETIS model was calibrated for the October 2007 event (the event to be

reconstructed), by adjusting its model parameters, and its performance was assessed for three other rainfall events (April 2003, October 2008 and September 2009) for the same station.

278

No evapotranspiration data was available for this study. Evapotranspiration is, along with soil characteristics and their relationships with soil saturation dynamics, acknowledged to be a key issue in the formation of flash floods in several studies (Braud et al., 2014, 2010; Nikolopoulos et al., 2011; Norbiato et al., 2008), because it determines the soil storage capacity (or soil abstraction capacity) at the beginning of the flood event. On the other hand, evapotranspiration is often negligible or almost negligible during the actual flood event. The lack of precise evapotranspiration data prevents from initializing the model state variables by means of a warm-up simulation. Thus, we decide to implement the model at the event scale. This means that the initial values of all state variables must be calibrated along with the model parameters for each flood event. In particular, the initial value of the soil static storage, which is a model state variable related to soil wetness, is a key variable for flash flood modeling, and must be calibrated carefully. The initial soil storage of the events used to calibrated the hydrological model (October 2007 for the first calibration and April 2003, October 2008 and September 2009 for the hydrological model evaluation) was adjusted along with the model parameters in order to reproduce the observed hydrograph at the Guadalest reservoir. The initial soil storage value was adjusted separately for each event.

296

The model calibrated at the Guadalest catchment was used to reproduce the October 2007 hydrograph of the Girona River upstream of the floodplain (indicated as the hydraulic model area in Figure 1). This was done by running the TETIS model for the

300 Girona River catchment with the parameterization obtained from the Guadalest
301 catchment. This process of extrapolation from a gauged catchment to an ungauged one
302 is widely used in distributed hydrological modeling (Vélez et al., 2009), and it is known
303 to amplify the uncertainty of the model result. For this reason, we used the extrapolated
304 model results to obtain only the hydrograph shape, while the actual magnitude of the
305 Girona River hydrograph was obtained by calibrating the initial soil storage and using
306 post-flood information as a reference. In particular, the initial soil storage was modified
307 within a reasonable range in order to obtain a set of hydrographs with the same shape
308 but different peak flows and volumes, which were used as boundary condition for a
309 flood model. A flood simulation was run with each of these hydrographs, the resulting
310 water depth maps were compared with post-flood information similarly to what was
311 done by Braud et al. (2010), and the simulation providing the best fit was selected. This
312 was done by comparing visually the observed and simulated flood zone. The final
313 October 2007 reconstructed hydrograph was the one returning the best fit between
314 observed and simulated inundation map and flood depths.

315

316 3.2. Hydraulic modeling

317

318 The set of hydrographs produced by the hydrological model were used as inlet
319 discharge to simulate the flooding event at the floodplain of the Girona River (Figure 1).
320 To that end, the free surface flow module of the model RiverFlow2D (Murillo and
321 García-Navarro, 2010; Lacasta et al., 2014) was used.

322

323 3.2.1. Hydraulic model

324

325 The 2D Shallow Water Equations, which express the water volume and momentum
326 conservation in x and y directions, were used in this work (Eq. 1):

327

$$328 \quad \frac{\partial}{\partial t} \begin{pmatrix} h \\ hu \\ hv \end{pmatrix} + \begin{pmatrix} hu \\ hu^2 + \frac{1}{2}gh^2 \\ huv \end{pmatrix} + \frac{\partial}{\partial y} \begin{pmatrix} hv \\ huv \\ hv^2 + \frac{1}{2}gh^2 \end{pmatrix} = \begin{pmatrix} 0 \\ -gh \left(\frac{\partial z}{\partial x} + S_{fx} \right) \\ -gh \left(\frac{\partial z}{\partial y} + S_{fy} \right) \end{pmatrix} (1)$$

329

330 Where h is the water depth, (u, v) are x and y averaged velocity components
331 respectively, z is the bottom level and the friction losses (S_f) are written in terms of
332 Manning's roughness coefficient (n) (Eq. 2):

333

$$334 \quad S_{fx} = \frac{n^2 u \sqrt{u^2 + v^2}}{h^{4/3}}, S_{fy} = \frac{n^2 v \sqrt{u^2 + v^2}}{h^{4/3}} (2)$$

335

336 In order to solve the system of equations, an upwind cell-centered finite volume model
337 was applied (Toro, 2001, Murillo and García-Navarro, 2010). The domain was
338 discretized into triangular cells and, assuming a piece wise representation of the
339 variables, an explicit first order Godunov (1959) method based on Roe's approach was
340 considered (Roe, 1981, Murillo and García-Navarro, 2010) (Eq. 3):

341

$$342 \quad U_i^{n+1} = U_i^n - \frac{\Delta t}{A_i} \sum_{k=1}^{NE} \sum_m^3 \left[(\tilde{\lambda} - \tilde{\nu} \tilde{e})_k^m l_k \right]^n (3)$$

343

344 where $U = (h, hu, hv)$ is the vector of conserved variables, NE indicates the number of
345 edges in cell i , l_k is the length of each edge k , $\tilde{\lambda}$ and \tilde{e} are the eigenvalues and
346 eigenvectors of the Jacobian matrix, respectively, and $\tilde{\nu}$ accounts for the linearized
347 fluxes and source terms expressed compactly (Morales-Hernández et al. 2013).

Moreover the numerical method was implemented in GPU architectures in order to accelerate the computations. More information can be found in Lacasta et al. (2014).

350

3.2.2. Topography

352

A Digital Terrain Model (DTM) of 1x1 m resolution derived from LiDAR (Light Detection and Ranging) data was used as base information to perform the final domain discretization. LiDAR data was collected in 2009 by the PNOA (The National Plan of Aerial Orthophotogrammetry, Government of Spain), using an Optech ALS50-II sensor, with a minimum laser pulse rate frequency of 45 kHz, a field of view angle of 50° and a scan rate of 70 Hz. The final density ranged between 0.5 (most of the area) and 2 points/m² (flight overlapping). Reported vertical and planimetric (X, Y) errors were lower than 40 and 36 cm, respectively. Then, a Digital Elevation Model (DEM) was performed using ground returns in Fusion software v3.30 (McGaughey, 2009). Likewise, a building map was carried out using the building returns in Fusion software v3.30 (McGaughey, 2009). Both models were combined to perform the DTM.

364

However, the following modifications of the DTM were carried out in order to represent accurately the simulated domain: i) as the LiDAR does not represent the terrain behind the bridges, this task was carried out manually using the nearest neighbour interpolation of ArcGis9.3 software (ESRI, Redlands CA); ii) introduction of the two pillars in CV-729 bridge as topographical element as they were not represented by the LiDAR iii) some buildings were removed from the building map as they did not exist in 2007; iv) agricultural walls and irrigation infrastructures were also modified in order to represent the terrain of 2007. Besides, some of them were not accurately reproduced by LiDAR

373 data, and were manually introduced; and v) riverbanks, gravel bars and ripraps were
374 also modified according to the topography of 2007. Finally the modified DTM is
375 discretized to perform an unstructured triangular mesh with 1,858,396 cells.

376

377 The roughness of the domain was defined depending on the land use, which was
378 obtained from the Corine map (European Environment Agency, 2007). The Manning
379 roughness coefficient was assigned to each habitat according to the recommendations
380 found in the specialized bibliography (i.e. Chow, 1959; Acrement and Schenider, 1990;
381 Rhee et al., 2008; González-Sanchis et al., 2012).

382

383 The inlet boundary condition was the hydrograph derived from the hydrological model.
384 On the contrary, the only outlet boundary condition was that of the sea level, which was
385 established following the tidal levels suggested by GIOC (2001).

386

387

388 3.3. Geomorphology and post-flood surveys

389

390 3.3.1. Geomorphologic works.

391

392 A geomorphologic survey of the study area was developed in order to assess and
393 reconstruct flood processes. This task was based on field surveys along the river and
394 throughout the whole Girona floodplain, topographic analysis through GIS and
395 geological maps interpretation (Vegas et al., 1975; Lendínez et al., 2008), so as to
396 identify geomorphological features and processes. Geomorphologic mapping was
397 developed using orthoimages (1:5,000) dating from 2007 (Instituto Geográfico

398 Nacional, IGN, www.cnig.es). Panchromatic black-and-white aerial photographs dating
 399 from 1946 (1:40,000) and 1956 (1:33,333) (Ministry of Defense, CECAF) were used to
 400 identify forms recently transformed by urban expansion processes. The photographs
 401 were scanned at a resolution of 400 dpi to obtain average pixel dimensions of 1 m and
 402 1.15 m respectively, and they were georeferenced to IGN orthophotos using ArcGIS
 403 TM version 9.3 (ESRI, Redlands, CA, 2009). The LiDAR-based DEM performed for
 404 hydraulic modeling was also used for topographic and geomorphologic analysis.

406 3.3.2. Flooded area

407
 408 The mapping of the flooded area was obtained from two different sources. First, some
 409 days after the flood, the external edge of the flooded area was surveyed using GPS.
 410 These data were exported to shape file format to be processed with ArcGISTM version
 411 9.3 (ESRI, Redlands, CA, 2009). This information was compared with a map composed
 412 by the Plataforma Ciutadana Riu Girona (PCRG) association. This organization was
 413 created by some citizens affected by the October 2007 flood, in order to promote
 414 research on this river basin and to prevent future floods. The PCRG collected
 415 information from both local administrations and witnesses to map the evolution of the
 416 flood, which was simulated through a video (PCRG, 2009, <https://vimeo.com/5487707>).
 417 Some small discrepancies were found between the GPS mapping and the PCRG video-
 418 mapping. Part of them was solved after visiting the area and consulting some members
 419 of the PCRG and other interviewed witnesses. Finally, the flooded area between
 420 Beniarbeig and El Verger was selected for evaluation, because it did not present
 421 significant discrepancies between the two sources and reproduced with the highest
 422 precision the flooding event (Figure 5).

423

424 3.3.3. Maximum flood depths.

425

426 The day after the flood, some technicians from the municipality of El Verger visited all
427 the buildings affected by the flood, in order to produce an assessment to be used to
428 calculate economic compensations for damages. Flood levels recorded by this report
429 were compared with flood marks observed in pictures taken by the authors or included
430 in the report, in order to correct some over-dimensioned records. A total of 64 points
431 with a register of the maximum flood depth were used to assess the performance of the
432 hydrological and the hydraulic model. These data are limited to the town of El Verger,
433 which represents only a small fraction of the total flooded area (Figures 5 and 6).

434

435 Table 1. Contrasted maximum flood depth marks in El Verger.

436

Id	Flood depth (m)	UTM		Street	Id	Flood depth (m)	UTM		Street
		x	y				x	y	
1	0,3	761256	4303653	Abadia	33	1,8	761354	4303776	Miraflor
2	0,3	761269	4303654	Abadia	34	1,6	761384	4303839	Miraflor
3	0,3	761269	4303649	Abadia	35	1,8	761352	4303761	Miraflor
4	0,7	760985	4303663	Calvari	36	1,8	761354	4303770	Miraflor
5	0,1	761032	4303670	Calvari	37	1,8	761345	4303716	Miraflor
6	1,7	761376	4303759	Xile	38	0,2	761504	4303905	Miraflor
7	1,5	761380	4303762	Xile	39	1,8	761344	4303707	Miraflor
8	1,3	761381	4303757	Xile	40	2,4	761288	4303585	Riu
9	0,1	761395	4303754	Xile	41	3	761290	4303584	Riu
10	0,1	761402	4303753	Xile	42	1,7	761363	4303887	Sant Isidre
11	0,1	761045	4303710	Constitució	43	0,3	761350	4304060	Sant Vicent
12	2,2	761301	4303711	Divina Aurora	44	0,25	761360	4304111	Sant Vicent
13	2,2	761308	4303814	Divina Aurora	45	0,3	761348	4304055	Sant Vicent
14	2,2	761310	4303842	Divina Aurora	46	0,25	761353	4304091	Sant Vicent
15	2,2	761311	4303850	Divina Aurora	47	0,3	761352	4304068	Sant Vicent
16	2,2	761308	4303821	Divina Aurora	48	0,2	761346	4304066	Sant Vicent
17	2,2	761301	4303704	Divina Aurora	49	0,2	761353	4304085	Sant Vicent
18	2,2	761309	4303831	Divina Aurora	50	0,25	761357	4304100	Sant Vicent
19	2,2	761301	4303716	Divina Aurora	51	0,1	761342	4304052	Sant Vicent
20	2,2	761299	4303727	Divina Aurora	52	1,8	761370	4303808	Santo Domingo
21	2,2	761310	4303857	Divina Aurora	53	1,6	761374	4303806	Santo Domingo

22	2,2	761299	4303730	Divina Aurora	54	1,6	761377	4303809	Santo Domingo
23	0,4	761230	4304266	Els Poblets	55	1,2	761388	4303804	Santo Domingo
24	1,7	761288	4303700	Forn	56	0,8	761391	4303797	Santo Domingo
25	0,1	761400	4303692	Girona	57	1,2	761387	4303799	Santo Domingo
26	0,1	761413	4303697	Girona	58	0,5	761395	4303801	Santo Domingo
27	0,3	761210	4304245	La Via	59	0,5	761396	4303793	Santo Domingo
28	0,1	761064	4304354	La Via	60	0,3	761402	4303791	Santo Domingo
29	1,8	761355	4303796	Miraflor	61	0,1	761410	4303788	Santo Domingo
30	1,8	761364	4303802	Miraflor	62	0,8	761332	4303639	Veneçuela
31	1,8	761375	4303821	Miraflor	63	0,8	761336	4303643	Veneçuela
32	1,8	761358	4303787	Miraflor	64	0,3	761336	4303638	Veneçuela

437

438

439 3.4 Evaluation of the simulated flooding event.

440

441 The results of the hydraulic model fed with the results of the hydrological model were
 442 evaluated using the post-flood surveys: maximum flooded area and flood depth. The
 443 observed maximum flood extension was compared to the estimated one following Bates
 444 and De Roo (2000) criteria, in which the accuracy of the calculated flood extent versus
 445 the observed is defined on:

446

$$447 \text{Fit}_A(\%) = \frac{FA_{obs} \cap FA_{mod}}{FA_{obs} \cup FA_{mod}} \times 100 \quad (4)$$

448

449 Where FIT_A is a goodness-of-fit index, and FA_{obs} and FA_{mod} are the observed and
 450 modelled flooded areas respectively. The observed and simulated maximum flood
 451 depths at the 64 points of El Verger are compared using the following goodness-of-fit
 452 indexes: Root Mean Square Error (RMSE) and Nash and Sutcliffe Efficiency - NSE
 453 (Nash and Sutcliffe, 1970).

454

455 3.5. Hydro-geomorphologic response to model simulations

456

457 Simulations varying flow conditions, with peak flows ranging from $150 \text{ m}^3 \text{ s}^{-1}$ to 900
458 $\text{m}^3 \text{ s}^{-1}$ with intervals of $10 \text{ m}^3 \text{ s}^{-1}$ were carried out to estimate the hydro-geomorphologic
459 response of the Girona River floodplain. The aim of these simulations was to identify
460 the threshold of activation for different geomorphic elements: alluvial fans, inter-fan
461 depressions, paleochannels and tectonic depressions, and to analyse the flood risk (and
462 how to prevent it) within the study area.

463

464 4. Results

465

466 4.1. Hydrological modeling

467

468 The hydrological model TETIS was calibrated at the Guadalest Reservoir flow gauge,
 469 by comparing the predicted and the observed water discharge. As explained in the
 470 methodology section, given that the model was implemented at the event scale, the
 471 initial state of soil moisture was unknown and was also calibrated. The results are
 472 shown in Figure 5. The model provided a NSE of 0.88. It was evaluated on different
 473 episodes, showing NSE of 0.88, 0.92 and 0.91 for the April 2003, October 2008 and
 474 September 2009 events respectively (different initial conditions of soil moisture were
 475 adjusted manually for each case), providing satisfactory results. More information about
 476 the TETIS model implementation can be found in Francés et al. (2011), CHJ (2012) and
 477 Bussi et al. (2012).

478

479 The October 2007 hydrograph of the Girona River was reconstructed using TETIS. A
 480 set of 26 hydrographs was generated (Figure 7) varying the initial soil storage from 35%
 481 to 60%, and it was used as the input of the flood model.

482

483 Table 2. – Characteristics of the reconstructed flood event (October 2007) for the
 484 Girona River catchment, following the results of the hydrological model.

485

Total precipitation – catchment average (mm)	343
Max rainfall intensity – catchment average (mm h ⁻¹)	69.5
Total rainfall volume (catchment) at the hydraulic model inflow section (Mm ³)	35.2

Total hydrograph volume (Mm^3)	11.2
Proportion of overland flow to total rainfall (%)	15.5
Proportion of interflow to total rainfall (%)	16.7
Maximum discharge($\text{m}^3 \text{s}^{-1}$)	515
Unit discharge($\text{m}^3 \text{s}^{-1} \text{km}^{-2}$)	0.58
Unit peak discharge($\text{m}^3 \text{s}^{-1} \text{km}^{-2}$)	5.0
Runoff coefficient (%)	31.9

486

487 The observed precipitation series showed two rainfall peaks. The first occurred between
 488 10:00 and 10:45, with maximum intensity over 100 mm h^{-1} in the headwaters (Ebo
 489 Valley). The second took place between 11:15 and 11:45 in the central part of the
 490 catchment, mainly at the southern part of Laguar Valley. Again, the rainfall intensity
 491 was above 100 mm h^{-1} . The average hyetographs describes well both peaks, with
 492 intensities above 69.5 mm h^{-1} (Figs. 4a and 4b).

493

494 According to the hydrological model results, the discharge at the catchment outlet
 495 (hydraulic model inflow) started to rise at 8:30AM (12th October) and reached a peak at
 496 13:00 ($515 \text{ m}^3 \text{s}^{-1}$) (Fig. 8). The hydrograph lag-time was established as the difference in
 497 time between the precipitation peaks (11:20 at Isbert and Carrasca and 11:40 at Alcalalí
 498 and Gallinera) and the peak discharge time. That provides a lag time of 1h20' – 1h40',
 499 which is typical for flash floods in similar catchments (Camarasa- Belmonte and
 500 Segura-Beltrán, 2001) and slightly higher than those estimated by Marchi et al (2010).

501

502 The flood lasted two days, although the largest discharges (above $100 \text{ m}^3 \text{s}^{-1}$) only took
 503 place during 8 hours and 40 minutes. Using the methodology detailed in Salazar et al.

(2013), the peak discharge return period was estimated to be 40 years, while the expected return period of daily rainfall was estimated to be slightly lower than 50 years. As expected, the single rainfall burst observed produced a single discharge peak. A second and smaller rainfall burst took place at 19:30 and produced a relatively reduced discharge peak ($150 \text{ m}^3 \text{ s}^{-1}$) at 21:00, repeating the 1-2 h lag time observed above.

4.2. Hydraulic modeling

The set of 26 hydrographs generated with the hydrological model varying the initial soil storage from 35% to 60% was used as input to the hydraulic model. The simulation results were analysed according to the post-flood survey information available and the geomorphology. Following this analysis, the hydrographs derived from the initial soil storage between 35 and 40 % showed a simulated flooded area smaller than the observed, likewise, initial soil storages higher than 45 %, causes a much larger flooded area than that occurred during the October 2007 event. Thus, the hydrographs obtained with initial soil storages between 35 and 40 %, and between 46 and 50 % were dismissed.

In order to select only one hydrograph that represented the flood of October 2007, the results of the hydrographs with initial soil storage between 41 and 45 % were analysed in detail by comparing the simulated and the observed maximum flooded area and flood depth (see Table 3). The comparison showed a good agreement between observed and simulated flooded area for the five hydrographs, whose Fit_A varied from 75.3 to 76.4 % (see Table 3). Likewise, the flood depth showed an acceptable accuracy, with a NSE

and RMSE that ranged between 0.58-0.61 and 0.64-0.69, respectively (see Table 3). All five hydrographs accurately reproduced the flooded area. However, the best compromise between flooded area and flood depth accuracy was that provided by the hydrograph generated with initial soil storage of 44 % (see Table 3 and Figure 9). Thus, according to the combination between hydrological and hydraulic modeling with post-flood information it can be stated that the flash flood occurred in October 2007 at the Girona River reached a peak discharge of $515 \text{ m}^3 \text{ s}^{-1}$.

Table 3. Results of the comparison between observed and estimated maximum flood depth (NSE and RMSE) and maximum flooded area (Fit_A) using the hydrographs derived from the initial soil storage between 41 and 45 %.

Initial soil storage (%)	41	42	43	44	45
NSE	0.58	0.59	0.59	0.60	0.61
RMSE	0.69	0.68	0.66	0.65	0.64
Fit_A	75.61	76.13	76.39	76.14	75.28

4.3. Floodplain geomorphologic configuration

The morphology and evolution of the systems of prograding fans is strongly related to flood dynamics. The complex configuration of the features of the fans system, the location of geomorphic elements -such as paleochannels, interfan depressions and intersection points-, and the fluvial scarp height, determine the activation or inactivity of the different portions of the fan system. Thus, in order to understand the relationship

550 between geomorphic units and flood processes, several morphological units have been
551 identified:

552

553 i) Middle Pleistocene fan (F1)

554

555 Downstream Beniarbeig, where the river valley widens, numerous avulsion processes
556 created a complex system of prograding alluvial fans, with different paleochannels
557 (Figure 10). The older fan (F1) has the apex beside the AP-7 Motorway and, according
558 to Vegas et al. (1975), was formed in the Middle Pleistocene. Another fan (F2) overlaps
559 part of this sediment body, dividing it into two portions: the Clot del Francés and the
560 Alberca sectors.

561

562 The area locally named Clot del Francés (literal translation: the Frenchman's Hollow)
563 lies on the left side. It is a corridor which is determinant for the Girona River flooding
564 processes, because it concentrates part of the overbank flow coming from the western
565 river bank, through the P3 and P4 paleochannels. The Cremadella Ravine, which also
566 flows into this corridor, forms a small torrential fan (F3) at the western side of the Clot
567 del Francés depression (Figure 10, 11a y 11b).

568

569 To the right, The Alberca Ravine flows through the external side of another fan sector,
570 attached to several Miocene hills. Two paleochannel are clearly identified in this area
571 (P1 and P2) (figure 11b). Due to the convexity of the fans surface, an inter-fan
572 depression is formed between fans F1 and F2, which can concentrate overbank flow
573 from Girona and Alberca channels (Fig. 10).

574

575 ii) Late Pleistocene fan

576

577 A prograding fan (F2), attributed to the Late Pleistocene by Vegas et al. (1975),
 578 overlaps the F1 fan (Figure 10). The apex is located upstream El Verger. Cross sections
 579 3 and 4 (Figure 11c and 11d) show the marked topographic convexity of this sediment
 580 body, in comparison with the F1 fan. Moreover, fan F2 is formed by several prograding
 581 lobes, with different paleochannels created through numerous avulsion processes. The
 582 intersection point IP1 is the apex of the dissymmetric lobe L1, well developed at the left
 583 bank. Immediately downstream El Verger, the river turns to the East, leaving a
 584 paleochannel (P5) to the North. At this point there is a crevasse splay, clearly marked at
 585 the microtopography, which presents an accumulation of boulders transported by the
 586 2007 flood (Figure 6c). Paleochannels P5 and P6 prologue the alluvial fan towards the
 587 coastline. Another lobe (L2) is developed from the intersection point IP2, at Els Poblets.
 588 It has also a paleochannel (P7), which flows towards the inter-fan depression. At the
 589 distal area of the F2 fan, a small Holocene alluvial fan (F6) forms the triangular shaped
 590 protuberance of the Almadrava Cape.

591

592 iii) Portelles fans

593

594 Girona River fans coalesce with deposits formed by the Portelles ravine (Figure 10).
 595 During floods, paleochannels can connect these systems. In fact, during the event that
 596 occurred in 2007, overbank flow from the Girona River was partially drained by the
 597 Portelles channel. The Portelles Ravine forms a small torrential fan at the foot of the
 598 Segària Mountain (F4). At the connection with the Clot del Francés paleochannel (P3),
 599 there is a wide fan, jointly built by the paleochannels of the Girona River and Portelles

600 ravine, in contact with the Pego-Oliva marsh. In its last reach, the channel almost
601 completely vanishes, and leaves a Holocene fan (F5) on this coastal marsh.

602

603 iv) Fluvial scarp

604

605 Fluvial scarp has 5 m depth in the F2 fanhead area, and 4 m between El Verger and the
606 F6 apex. From this point, the fluvial scarp markedly decreases until disappearing at the
607 river mouth. The river banks are markedly dissymmetric (Figure 12). The right one is
608 higher than the left one in most of the study area. This favours overbank flow on the left
609 bank of the fan system. Figure 12 also shown the critical effect generated by the silted
610 weir of the historical water mill of Alcovir, which artificially reduces the depth of the
611 fluvial scarp, facilitating overbank flow towards the P3 paleochannel.

612

613 v) Human floodplain occupation and impacts on the river channel

614

615 Valencian floodplains have been largely urbanized during the last four decades. In the
616 Girona River basin, the historical villages grew over the fans, terraces and point-bars. In
617 the El Verger urban area, some of the houses located on the left bank of the Girona
618 River narrowed the river section before the 2007 flood. After 1970, touristic residences
619 were massively built on the coastal area. This urbanized sector altered the original
620 topography of P5 and P6, facilitating overbank flow dispersion. Besides, over the
621 floodplain, several irrigation canals and walls built for agricultural or industrial
622 purposes protect some areas from floods, partially altering flow distribution in the Clot
623 del Francés (P3) area.

At the river channel, as explained above, the impact of the Molí d'Alcovir weir is also remarkable. This weir alters the slope of the river talweg (Figures 12 and 13). Moreover, numerous bridges cross the river channel in the study area, but most of them, placed in urban channelized reaches, do not modify significantly the river section (Figure 13). The only exception in the model area is the CV-729 bridge, which reduces the trapezoidal section of the river channel from 82.26.m² to a 58.52 m² rectangular section. The AP-7 motorway bridge is high and wide, however, the height of this infrastructure, artificially raised, can act as a dike for overbank flow.

4.4. Flooding thresholds for morphological units

Hydro-geomorphological responses for different flow conditions were estimated through various simulations. Results (Table 4, Figure 9) showed an activation sequence for paleochannels and alluvial fans, altered by the Clot del Francés depression (P7) and the impact of the CV-729 Bridge, in the Motorway A-7.

Table 4. Flooding thresholds for geomorphologic units

<i>Flow (m³ s⁻¹)</i>	<i>Effects</i>	<i>Fans Activation</i>
190	No impact on point-bars or paleochannels. Overbank flow at river mouth meander, immediately upstream F6 .	F6 (Holocene)
300	Point-bars flooded. Crevasse splay and P5 and P6 initial activation.	L1 in F2 (Late Pleistocene)
350	Overbank flow from IP2 left bank (Els Poblets) to P5	L2 in F2 (Late Pleistocene)
360	P3 (Clot del Francés) initial activation.	Left side of F1 (Middle Pleistocene)

400	Initial overbank flow at P4 . Overbank flow at L2 over F2 distal area.	
515	Optimal coincidence between flooded area and hydraulic model.	F5 (Holocene, Portelles Ravine)
527	P7 initial activation.	
590	P7 active. Overbank flow from IP2 right bank also flooding the inter-fan depression.	Inter-fan depression
610	Initial overbank flow at Beniarbeig	Bajada
640	AP7 motorway creating stagnation effect on overbank flow from Beniarbeig	
650	Return flow from P4 to Girona River at the beginning of the urban area of El Verger (immediately upstream IP1)	
670	Initial overbank flow on the right side of CV-729 Bridge.	Right side of F1 (Middle Pleistocene)
800	Overbank flow on the right bank at the beginning of El Verger urban area (immediately upstream IP1)	

642

643

644

645 5. Discussion

646

647 The hydrological model provided a high unit peak discharge of $5.0 \text{ m}^3 \text{ s}^{-1} \text{ km}^2$. For the
648 Spanish Mediterranean, Gaume et al. (2009) found a maximum unit peak discharge of
649 around $10 \text{ m}^3 \text{ s}^{-1} \text{ km}^2$ for a 100 km^2 catchment. The Girona River unit peak discharge
650 for the October 2007 event is also within the range of peak discharge data collected by
651 Marchi et al. (2010). The ratio of the unit peak discharge ($5 \text{ m}^3 \text{ s}^{-1} \text{ km}^2$) and the unit
652 average discharge ($0.58 \text{ m}^3 \text{ s}^{-1} \text{ km}^2$) is 8.65. Given the outcomes of these studies, the
653 October 2007 can be classified as an extreme rainfall event whose magnitude is very

654 close to the unit peak discharge envelope curve showed by Gaume et al. (2009) and
655 Marchi et al. (2010).

656

657 In this study, we calculated a runoff coefficient of 0.319 (Table 2). This is similar to
658 what was found by Marchi et al. (2010). These authors analysed 25 flash floods in
659 Europe and found that the mean value is 0.35, with standard deviation equal to 0.18,
660 median value 0.37 and 0.20-0.45 interquartile range. However, the value found in the
661 present study is substantially higher than the runoff coefficients found by Goodrich
662 (1990) who analysed five large flash floods events at the semi-arid catchment of Walnut
663 Gulch (US) occurred within a 20-year period and found runoff coefficients between
664 0.07 and 0.21. Segura-Beltrán (1990) and Camarasa-Belmonte and Segura-Beltrán
665 (2001) found that, in other limestone catchments of the Valencia region, for a 25-year
666 time series and 35 floods, the runoff coefficients were between 0.007 and 0.16. These
667 values, observed in karstified limestone catchments, indicate that the infiltration is
668 relatively high, as well as the initial abstractions and the soil retention. The catchments
669 can infiltrate a large amount of water, and when they are saturated they produce a
670 sudden pulse of runoff (Camarasa-Belmonte and Segura-Beltrán, 2001).

671

672 Simulated and observed maximum flooded area and flood depth were compared in order
673 to adjust the hydrograph. This comparison showed the accuracy of the model predicting
674 the maximum flooded area (see the goodness-fit indicator Fit_A in Table 3), which is a
675 good test of model capabilities and is of a significant practical interest (Bates and De
676 Roo, 2000). The goodness-fit indicator Fit_A reached 76.14 %, and is similar to that
677 reported by González-Sanchis et al. (2012) using the same hydraulic model, which
678 ranged from 64 to 92 %. The resulted accuracy is also comparable to other studies, such

679 as Horritt and Bates (2001), who obtained a $\text{Fit}_A = 0.84\%$ or Tayefi et al (2007) who
680 reported a Fit_A between 51 and 65 %.

681

682 Regarding the evaluation of the maximum flood depth, the results showed an acceptable
683 accuracy, although slightly lower than the one reported in other studies (Connell et al.
684 (2001), Erpicum et al. (2010), Büttner et al. (2006)). However, the lower accuracy
685 registered in this study could be due to the fact that none of these studies simulate the
686 whole flooding event, but only steady-state peak flows. González-Sanchis *et al* (2012)
687 simulated five transient flooding events using the same hydraulic model and obtained a
688 slightly higher accuracy than the one reported in this study. Thus, our lower accuracy
689 might not only be due to the transient characteristics of the simulated flood, but also to
690 the high complexity of the case. Unlike the cited studies, this study is highly complex in
691 terms of simulation and event reconstruction, as the Girona River is ephemeral,
692 ungauged, the inlet discharge was estimated from a hydrological model and the outlet
693 discharge was unknown.

694

695 With regard to the flooding processes, alluvial fan systems have flood-hazardous
696 conditions due to their convex topography, which creates high flow direction
697 uncertainty downstream the intersection point (and/or fan apex). The determination of
698 the active zone (area where flooding, erosion, and sedimentation are possible) of these
699 alluvial forms is a complex task, which can be solved with the combination of
700 hydrologic, hydraulic and geomorphologic techniques. Several authors have addressed
701 this topic with different approaches. Santangelo et al. (2012), in their analysis of fan
702 systems, considered as active zone all the fan portions located down-fan of the
703 intersection point. This is consistent with the NRC (1996) recommendations, which

704 followed a geo-chronological criterion, considering the Holocene fans as the most active
705 zones.

706

707 Moreover, Segura-Beltrán (2003) showed that, in the Valencia Region coastal plains,
708 the topographic complexity of alluvial fans structure requires a more detailed analysis,
709 in order to discriminate between morphological units with different flood-hazard. In
710 these contexts, the activation of paleochannels and the presence of inter-fan depressions
711 play a major role during flood events. During the Girona 2007 flash flood,
712 paleochannels conveyed an important proportion of the overbank flow, preventing other
713 areas of the alluvial fans from flooding, as it was shown in the real event and model
714 simulations. Besides, inter-fan depressions should be also considered as active zones,
715 due to its capability to drain flow from both the fan distal areas and the paleochannels,
716 as it is shown in simulations with stream flow $> 600 \text{ m}^3 \text{ s}^{-1}$.

717

718 In this work, the simulation of different flow conditions showed various thresholds for
719 fans flooding and paleochannels activation (Figure 9). In this fan system, throughfan
720 trenching and progradation difficult the interpretation of the flooding processes.

721 Along the Girona fan system throughfan trenching has been observed, and the fluvial
722 scarp is deeper in the fan Pleistocene areas than in the Holocen fans (Figure 12).

723 Throughfan trenching and lobes progradation creates a geochronological flood
724 sequence, causing first the activation of the Holocene sector, subsequently the Late
725 Pleistocene fan (F2), and finally the Middle Pleistocene areas (F1).

726

727 The lower flooding thresholds were located both at the point-bar areas and the Holocene
728 fan (F6). IP3 played a major role in F6 activation and the whole area downstream this

729 point –where the fluvial scarp is between 1 and 3 m– was flooded in the $350 \text{ m}^3 \text{ s}^{-1}$
 730 simulation. For these reasons, the Holocene fan should be considered as an active area.
 731 Inside each of Pleistocene units (F1 and F2), other factors –natural and anthropogenic--
 732 determine the activation of the different elements of the fan system. Regarding the
 733 natural factors, palaeochannels seem to be more relevant than intersection points. Thus,
 734 P5 is activated at $300 \text{ m}^3 \text{ s}^{-1}$, before overbank flow takes place at IP2 ($350 \text{ m}^3 \text{ s}^{-1}$), and
 735 P3 ($360 \text{ m}^3 \text{ s}^{-1}$) before than IP2 (Table 4 and Figure 14).
 736
 737 Moreover, some human-induced factors contribute to enhance overbank flow in several
 738 river reaches, such as: i) the effect generated by the silted weir of Molí d’Alcovir, which
 739 facilitates overbank flow towards the P3 paleochannel and ii) the effect of the CV-732
 740 bridge, which artificially narrows the river section, prematurely activating the P4
 741 paleochannel and also causing unexpected overbank flow activating the highest reach of
 742 the inter-fan depression beyond the $670 \text{ m}^3 \text{ s}^{-1}$ (Figure 14 c). Besides, other human
 743 infrastructures, such as walls and roads, alter the overbank flow on the fan surface
 744 (Figure 14).
 745
 746 It should be underlined that the Alberca sector of the Middle Pleistocene fan (F2) was
 747 not activated by any of the simulations launched. It is the only feature that should be
 748 considered as an inactive fan in this complex fan system, whereas the F2 and the Clot
 749 del Frances depression should be considered as quiescent areas.
 750
 751 In this regard, the urban use of some of these morphologies is considerably increasing
 752 exposure to floods in the area. While the older part of urban areas (previous to 1950)
 753 were in most cases not affected by the 2007 flash flood, recent constructions occupy

sensitive zones such as point-bars or paleochannels. The massive occupation of the coastal front blocks the flow descending to the Sea. For these reasons, the role played by the Clot del Frances paleochannel (P3) during this flash flood and the simulated scenarios demands the preservation of this area, free of constructions, for flood attenuation.

6. Conclusions

The analysis of the flash flood of the Girona River in 2007 has reconstructed the flooding susceptibility of this Mediterranean alluvial floodplain. From a methodological point of view, this integrated perspective is be a useful strategy for ungauged drainage basins. The combination of hydrologic and hydraulic modeling, and geomorphologic information allows understanding and generalizing the mechanisms governing floods in alluvial fans.

The implementation of both hydrologic and hydraulic models was complex in terms of simulation and evaluation, as this river is ephemeral and ungauged, but results are consistent with similar works. The interaction of the hydraulic model with the geomorphologic information was determinant to decipher flooding processes and to provide a better understanding of overlapping alluvial fan systems response. Results from this multidisciplinary research are a useful tool to perform risk prevention works and may be effectively used by the public administrations for early warning and risk mitigation purposes.

779

780 Acknowledgements

781

782 This collaborative research was financed with the projects CGL2013-44917-R and
783 SLWAMED CGL2014-58127-C3-2, of the Ministry of Economy and Competitiveness
784 of the Spanish Government. Both projects were co-financed with FEDER funds. The
785 observed rainfall and water discharge records were provided by “Sistema Automático
786 de Información Hidrológica (SAIH)”, which belongs to the CHJ (Spain). This work was
787 also possible due to the kind cooperation of the members of the Plataforma Ciudadana
788 Riu Girona and several anonymous farmers interviewed during the field works. We also
789 thank two anonymous reviewers for their useful and thought-provoking comments.

790

791

792

793 References

794

795 Acrement, G. C., Schenider, V. R. 1990. Guide for selecting Manning’s roughness
796 coefficients for natural channels and flood plains. Water-Supply Paper No. 2339, Dept.
797 of the Interior, U. S. Geological Survey, Reston, VA.

798 Anquetin, S., Braud, I., Vannier, O., Viallet, P., Boudevillain, B., Creutin, J.D., Manus,
799 C., 2010. Sensitivity of the hydrological response to the variability of rainfall fields and
800 soils for the Gard 2002 flash-flood event. J. Hydrol. 394 (1), 134–147.
801 doi:10.1016/j.jhydrol.2010.07.002

- 802 Armengot, R., 1994. Les precipitacions extraordinàries, in Pérez Cueva, A. (coord.)
803 Atlas Climàtic de la Comunitat Valenciana, COPUT, Generalitat Valenciana, Valencia,
804 pp. 98-99. (in Valencian).
- 805 Barredo, J.I., 2007. Major flood disasters in Europe: 1950–2005. *Natural Hazards* 42
806 (1), 125–148.
- 807 Barrera, A., Llasat, M., Barriendos, M., 2006. Estimation of extreme flash flood
808 evolution in Barcelona County from 1351 to 2005. *Natural Hazards and Earth System*
809 *Science*. 6 (4), 505-518.
- 810 Bates, P. D., De Roo, A. P. J. 2000. A simple raster-based model for flood inundation
811 simulation. *Journal of hydrology*, 236 (1), 54-77.
- 812 Bates, P.D., Wilson, M.D., Horritt, M.S., Mason, D.C., Holden, N., Currie, A., 2006.
813 Reach scale floodplain inundation dynamics observed using airborne synthetic aperture
814 radar imagery: Data analysis and modelling. *J. Hydrol.* 328 (1), 306–318.
815 doi:10.1016/j.jhydrol.2005.12.028.
- 816 Borga, M., Boscolo, P., Zanon, F., Sangati, M., 2007. Hydrometeorological Analysis of
817 the 29 August 2003 Flash Flood in the Eastern Italian Alps. *J. Hydrometeorol.* **8**, 1049–
818 1067. doi:10.1175/JHM593.1.
- 819 Borga, M., Anagnostou, E. N., Blöschl, G., & Creutin, J. D., 2011. Flash flood
820 forecasting, warning and risk management: the HYDRATE project. *Environmental*
821 *Science & Policy*, 14(7), 834-844.

- 822 Borga, M., Morin, E., 2014. Characteristics of Flash Flood Regimes in the
 823 Mediterranean Region, in: *Storminess and Environmental Change* (pp. 65-76). Springer
 824 Netherlands.
- 825 Braud, I., Roux, H., Anquetin, S., Maubourguet, M.M., Manus, C., Viallet, P., Dartus,
 826 D., 2010. The use of distributed hydrological models for the Gard 2002 flash flood
 827 event: Analysis of associated hydrological processes. *Journal of Hydrology*. 394 (1),
 828 162-181. doi:10.1016/j.jhydrol.2010.03.033.
- 829 Braud, I., Ayral, P.-A., Bouvier, C., Branger, F., Delrieu, G., Le Coz, J., Nord, G.,
 830 Vandervaere, J.-P., Anquetin, S., Adamovic, M., Andrieu, J., Batiot, C., Boudevillain,
 831 B., Brunet, P., Carreau, J., Confoland, A., Didon-Lescot, J.-F., Domergue, J.-M.,
 832 Douvinet, J., Dramais, G., Freydier, R., Gérard, S., Huza, J., Leblois, E., Le Bourgeois,
 833 O., Le Boursicaud, R., Marchand, P., Martin, P., Nottale, L., Patris, N., Renard, B.,
 834 Seidel, J.-L., Taupin, J.-D., Vannier, O., Vincendon, B., Wijbrans, A. 2014. Multi-scale
 835 hydrometeorological observation and modelling for flash-flood understanding.
 836 *Hydrology and Earth System Sciences*, 18(9), 3733-3761.
- 837 Buendia, C., Bussi, G., Tuset, J., Vericat, D., Sabater, S., Palau, A., Batalla, R.J., 2015.
 838 Effects of afforestation on runoff and sediment load in an upland Mediterranean
 839 catchment. *Sci. Total Environ.* 540, 144–157. doi:10.1016/j.scitotenv.2015.07.005
- 840 Bussi, G., Francés, F., Salinas, J.L., García-Bartual, R., Pujol, L., Ortíz, E., 2012.
 841 Estimación de mapas de peligrosidad mediante generación de tormentas sintéticas, in:
 842 Murillo Muñoz, R.E. (Ed.), *XXV Congreso Latinoamericano de Hidráulica*. Colegio de
 843 Ingenieros Civiles de Costa Rica, San José, Costa Rica (on CD). ISBN: 978-9968-933-
 844 06-3. (In Spanish).

- 845 Büttner, O., Otte-Witte, K., Krüger, F., Meon, G., Rode, M., 2006. Numerical
846 modelling of floodplain hydraulics and suspended sediment transport and deposition at
847 the event scale in the middle river Elbe, Germany. *Acta Hydrochim.Hydrobiol.* 34 (3),
848 265-278.
- 849 Camarasa-Belmonte, A.M., Segura-Beltrán, F.S., 2001. Flood events in Mediterranean
850 ephemeral streams (ramblas) in Valencia region, Spain. *Catena.* 45 (3), 229-249.
- 851 Camarasa-Belmonte, A.M., Soriano-García, J., 2012. Flood risk assessment and
852 mapping in peri-urban Mediterranean environments using hydrogeomorphology.
853 Application to ephemeral streams in the Valencia region (eastern Spain). *Landscape*
854 *Urban Plann.* 104, 189-200. doi: 10.1016/S0341-8162(01)00146-1
- 855 CHJ - Confederación Hidrográfica del Júcar, 2012. Plan director de defensa contra las
856 avenidas en la comarca de la Marina Alta (Alicante). Apéndice 6. Estudio hidrológico,
857 Valencia, Jucar River Basin Authority, 270. (In Spanish).
- 858 Chow, V.T., 1959. *Open-channel hydraulics*, New York, McGraw-Hill, 680.
- 859 Connell, R.J., Painter, D.J., Beffa, C., 2001. Two-dimensional flood plain flow. II:
860 Model validation. *J.Hydrol.Eng.* 6 (5), 406-415.
- 861 Creutin, J. D., Borga, M., Grunfest, E., Lutoff, C., Zoccatelli, D., & Ruin, I. (2013). A
862 space and time framework for analyzing human anticipation of flash floods. *Journal of*
863 *Hydrology*, 482, 14-24.doi:10.1016/j.jhydrol.2012.11.009
- 864 Di Baldassarre, G., Schumann, G., Bates, P.D., 2009. A technique for the calibration of
865 hydraulic models using uncertain satellite observations of flood extent. *Journal of*
866 *Hydrology.* 367 (3), 276-282. doi:10.1016/j.jhydrol.2009.01.020

- 867 Erpicum, S., Dewals, B., Archambeau, P., Detrembleur, S., Piroton, M., 2010. Detailed
 868 inundation modelling using high resolution DEMs. *Engineering Applications of*
 869 *Computational Fluid Mechanics*. 4(2), 196-208.
- 870 EEA - European Environment Agency, 2007. CLC 2006 technical guidelines. EEA
 871 Technical Report No 17/2007. European Environment Agency, Copenhagen.
- 872 Francés, F., Velez, J.I., Vélez, J.J., 2007. Split-parameter structure for the automatic
 873 calibration of distributed hydrological models. *Journal of Hydrology*. 332 (1), 226-240.
 874 doi:10.1016/j.jhydrol.2006.06.032
- 875 Francés, F., García-Bartual, R., Bussi, G., 2011. High return period annual maximum
 876 reservoir water level quantiles estimation using synthetic generated flood events, in:
 877 Escuder-Bueno, I., Matheu, E., Altarejos-García, L., Castillo-Rodríguez, J. (Eds.), *Risk*
 878 *Analysis, Dam Safety, Dam Security and Critical Infrastructure Management*.
 879 *Proceedings of the 3rd International Forum on Risk Analysis, Dam Safety, Dam*
 880 *Security and Critical Management (3IWRDD-FORUM)*, Valencia, Spain, 17-18
 881 October 2011. CRC Press, London, pp. 185–190.
- 882 Gaume, E., Bain, V., Bernardara, P., Newinger, O., Barbuc, M., Bateman, A.,
 883 Blaškovičová, L., Blöschl, G., Borga, M., Dumitrescu, A., Daliakopoulos, I., Garcia, J.,
 884 Irimescu, A., Kohnova, S., Koutroulis, A., Marchi, L., Matreata, S., Medina, V.,
 885 Preciso, E., Sempere-Torres, D., Stancalie, G., Szolgay, J., Tsanis, I., Velasco, D.,
 886 Viglione, A., 2009. A compilation of data on European flash floods. *Journal of*
 887 *Hydrology*. 367 (1), 70-78. doi:10.1016/j.jhydrol.2008.12.028

- 888 Gaume, E., Borga, M. (2008). Post-flood field investigations in upland catchments after
889 major flash floods: proposal of a methodology and illustrations. *Journal of flood risk*
890 *management*, 1(4), 175-189.doi:10.1111/j.1753-318X.2008.00023.x
- 891 GIOC, 2001. Atlas de inundación del litoral peninsular español. Grupo de Ingeniería
892 Oceanográfica y de Costas, Universidad de Cantabria (Spain) - Ministerio de Medio
893 Ambiente, Dirección General de Costas (Spain).59 pp. (in Spanish).
- 894 Godunov, S.K., 1959. A difference method for numerical calculation of discontinuous
895 solutions of the equations of hydrodynamics. *Matematicheskii Sbornik*. 89(3), 271-306.
- 896 González-Sanchis, M., Murillo, J., Latorre, B., Comín, F., García-Navarro, P., 2012.
897 Transient two-dimensional simulation of real flood events in a Mediterranean
898 floodplain. *J.Hydraul.Eng.* 1380 (7), 629-641.
- 899 Goodrich, D.C. 1990. Geometric simplification of a distributed rainfall-runoff model
900 over a range of basin scales, Ph. D. Thesis, University of Arizona, 361 pp.
- 901 Hall, J.W., Tarantola, S., Bates, P.D., Horritt, M.S., 2005. Distributed Sensitivity
902 Analysis of Flood Inundation Model Calibration. *J. Hydraul. Eng.*
903 doi:10.1061/(ASCE)0733-9429(2005)131:2(117).
- 904 Harvey, A. M., 2002. Effective timescales of coupling within fluvial systems.
905 *Geomorphology* 44 (3), 175-201.
- 906 Harvey, 2012. The coupling status of alluvial fans and debris cones: a review and
907 synthesis. *Earth Surf. Process. Landf.* 37 (1), 64-76. doi: 10.1002/esp.2213.

- 908 Horritt, M., Bates, P., 2001. Predicting floodplain inundation: raster-based modelling
909 versus the finite-element approach. *Hydrol. Process.* 15 (5), 825-842.
- 910 House, P.K., Baker, V.R., 2001. Paleohydrology of flash floods in small desert
911 watersheds in western Arizona. *Water Resour. Res.* 37 (6), 1825-1839.
912 doi:10.1029/2000WR900408.
- 913 Lacasta, A., Morales-Hernández, M., Murillo, J., García-Navarro, P., 2014. An
914 optimized GPU implementation of a 2D free surface simulation model on unstructured
915 meshes. *Adv.Eng.Software.* 78, 1-15.
- 916 Lara, A., Saurí, D., Ribas, A., Pavón, D., 2010. Social perceptions of floods and flood
917 management in a Mediterranean area (Costa Brava, Spain). *Natural Hazards and Earth*
918 *System Sciences.* 10 (10), 2081-2091. doi:10.5194/nhess-10-2081-2010
- 919 Lendínez, A., Muñoz, J.L., Pascual, H. 2008. Mapa Geológico de España. Benissa. Hoja
920 822. Memoria y cartografía. IGME, Madrid. (in Spanish).
- 921 Llasat, M.C., Marcos, R., Llasat-Botija, M., Gilabert, J., Turco, M., Quintana-Seguí, P.,
922 2014. Flash flood evolution in North-Western Mediterranean. *Atmos. Res.* 149, 230–
923 243. doi:10.1016/j.atmosres.2014.05.024
- 924 Marchi, L., Borga, M., Preciso, E., Gaume, E., 2010. Characterisation of selected
925 extreme flash floods in Europe and implications for flood risk management. *Journal of*
926 *Hydrology.* 394 (1), 118-133. doi:10.1016/j.jhydrol.2010.07.017
- 927 Martin-Vide, J., 2004. Spatial distribution of a daily precipitation concentration index in
928 peninsular Spain. *Int.J.Climatol.* 24 (8), 959-971

- 929 McGaughey, R., 2009. FUSION/LDV: Software for LIDAR data analysis and
930 visualization. US Department of Agriculture, Forest Service, Pacific Northwest
931 Research Station: Seattle, WA, USA. 123.
- 932 Morales-Hernández, M., García-Navarro, P., Burguete, J., Brufau, P., 2013. A
933 conservative strategy to couple 1D and 2D models for shallow water flow simulation.
934 Comput.Fluids. 81, 26-44.
- 935 Murillo, J., García-Navarro, P., 2010. Weak solutions for partial differential equations
936 with source terms: Application to the shallow water equations. Journal of
937 Computational Physics. 229 (11), 4327-4368.
- 938 Nanson, G.C., Tooth, S., Knighton, A.D., 2002. A global perspective on dryland rivers:
939 perceptions, misconceptions, and distinctions, in: Bull, L.J., Kirkby, M.J. (Eds.),
940 Dryland Rivers: Hydrology and Geomorphology of Semiarid Channels. John Wiley and
941 Sons, New York, pp. 17–54.
- 942 Nash, J., Sutcliffe, J.V., 1970. River flow forecasting through conceptual models part
943 I—A discussion of principles. Journal of hydrology. 10 (3), 282-290. doi:10.1016/0022-
944 1694(70)90255-6
- 945 NRC - National Research Council. Committee on Alluvial Fan Flooding, 1996. Alluvial
946 fan flooding, Washington, D.C., National Academy Press.
- 947 Nikolopoulos, E.I., Anagnostou, E.N., Borga, M., Vivoni, E.R., Papadopoulos, A.,
948 2011. Sensitivity of a mountain basin flash flood to initial wetness condition and rainfall
949 variability. J. Hydrol. 402(3), 165-178. doi:10.1016/j.jhydrol.2010.12.020

- 950 Norbiato, D., Borga, M., Degli Esposti, S., Gaume, E., Anquetin, S., 2008. Flash flood
951 warning based on rainfall thresholds and soil moisture conditions: An assessment for
952 gauged and ungauged basins. *Journal of Hydrology*. 362(3), 274-290.
953 doi:10.1016/j.jhydrol.2008.08.023
- 954 Pappenberger, F., Beven, K., Horritt, M., Blazkova, S., 2005. Uncertainty in the
955 calibration of effective roughness parameters in HEC-RAS using inundation and
956 downstream level observations. *J. Hydrol.* 302(1), 46-69.
957 doi:10.1016/j.jhydrol.2004.06.036
- 958 Pappenberger, F., Frodsham, K., Beven, K., Romanowicz, R., Matgen, P., 2007. Fuzzy
959 set approach to calibrating distributed flood inundation models using remote sensing
960 observations. *Hydrol. Earth Syst. Sci.* 11(2), 739-752 doi:10.5194/hess-11-739-2007
- 961 Pastor, F., Gómez, I., Estrela, M., 2010. Numerical study of the October 2007 flash
962 flood in the Valencia region (Eastern Spain): the role of orography. *Nat Hazards Earth*
963 *Syst Sci.* 10, 1331-1345. doi:10.5194/nhess-10-1331-2010
- 964 PCRG - Plataforma Ciutadana Riu Girona. 2009. Simulación de la riada del Girona de
965 2007, <https://vimeo.com/5487707> [accessed on 11/001/2016]. (In Spanish).
- 966 Pilgrim, D. H., Chapman, T. G., Doran, D. G., 1988. Problems of rainfall-runoff
967 modelling in arid and semiarid regions. *Hydrological Sciences Journal*, 33 (4), 379-
968 400. doi:10.1080/02626668809491261
- 969 Rhee, D.S., Woo, H., Kwon, B., Ahn, H.K., 2008. Hydraulic resistance of some selected
970 vegetation in open channel flows. *River research and applications*. 24 (5), 673-687.

- 971 Rodríguez-Lloveras, X., Bussi, G., Francés, F., Rodríguez-Caballero, E., Solé-Benet,
972 A., Calle, M., Benito, G., Rodríguez-Lloveras, X., Bussi, G., Francés, F., Rodríguez-
973 Caballero, E., Solé-Benet, A., Calle, M., Benito, G., 2015. Patterns of runoff and
974 sediment production in response to land-use changes in an ungauged catchment. *J.*
975 *Hydrol.* 531, 1054–1066. doi:10.1016/j.jhydrol.2015.11.014
- 976 Roe, P.L., 1981. Approximate Riemann solvers, parameter vectors, and difference
977 schemes. *Journal of computational physics.* 43(2), 357-372.
- 978 Salazar, S., Francés, F., Komma, J., Blume, T., Francke, T., Bronstert, A., Blöschl, G.,
979 2013. A comparative analysis of the effectiveness of flood management measures based
980 on the concept of "retaining water in the landscape" in different European hydro-
981 climatic regions. *Natural Hazards and Earth System Science.* 12, 3287-3306.
982 doi:10.5194/nhess-12-3287-2012
- 983 Santangelo, N., Daunis-i-Estadella, J., Di Crescenzo, G., Di Donato, V., Faillace, P.,
984 Martín-Fernández, J., 2012. Topographic predictors of susceptibility to alluvial fan
985 flooding, Southern Apennines. *Earth Surf.Process.Landforms.* 37 (8), 803-817.
- 986 Saxton, K.E., Rawls, W.J., 2006. Soil Water Characteristic Estimates by Texture and
987 Organic Matter for Hydrologic Solutions. *Soil Sci. Soc. Am. J.* 70(5), 1569-1578.
988 doi:10.2136/sssaj2005.0117
- 989 Schumann, G., Bates, P.D., Horritt, M.S., Matgen, P., Pappenberger, F., 2009. Progress
990 in integration of remote sensing-derived flood extent and stage data and hydraulic
991 models. *Rev. Geophys.* 47 (4). doi:10.1029/2008RG000274

- 992 Segura-Beltrán, F., 1990. Las ramblas valencianas: algunos aspectos de hidrología,
 993 geomorfología y sedimentología. Universitat de València, València, p. 229. (In
 994 Spanish).
- 995 Segura-Beltrán, F., 2003. Model d'inundacions en ventalls al·luvials: el cas de les planes
 996 costaneres valencianes. Cuadernos de Geografía, 73-74, 207-232. (In Catalan)
- 997 Segura-Beltrán, F., 2009. Geomorfología, inundaciones y alteración antrópica del
 998 espacio inundable: el caso del riu Girona (Alacant, octubre de 2007). Boletín de la
 999 Asociación de Geógrafos Españoles., 83-103. (In Spanish).
- 1000 Tayefi, V., Lane, S., Hardy, R., Yu, D., 2007. A comparison of one-and
 1001 two-dimensional approaches to modelling flood inundation over complex upland
 1002 floodplains. Hydrol.Process. 21(23), 3190-3202.
- 1003 Toro, E.F. 2001. Shock-Capturing Methods for Free-Surface Shallow Flows. Wiley,
 1004 New York, p. 109.
- 1005 Vegas, R.; Pedraza, J; Zazo, C; Goy, J. L.; Cabañas, J.; Uralde, M. A., 1975. Mapa
 1006 Geológico de Gandia. Hoja 796. Memoria y cartografía. IGME, Madrid. (In Spanish).
- 1007 Vélez, J.J., Francés, F., 2005. Automatic calibration of initial state variables for flood
 1008 forecasting using a distributed model. Int. Conf. Innov. Adv. Implement. Flood
 1009 Forecast. Technol. 17 to 19 Oct. 2005, Tromsø, Norw.
- 1010 Vélez, J.J., Puricelli, M., López Unzu, F., Francés, F., 2009. Parameter extrapolation to
 1011 ungauged basins with a hydrological distributed model in a regional framework.
 1012 Hydrology and earth system sciences. 13(2), 229-246. doi:10.5194/hess-13-229-2009

1013 Yatheendradas, S., Wagener, T., Gupta, H., Unkrich, C., Goodrich, D., Schaffner, M.,
1014 Stewart, A., 2008. Understanding uncertainty in distributed flash flood forecasting for
1015 semiarid regions. Water Resour.Res. 44 (5). doi:10.1029/2007WR005940

1016

ACCEPTED MANUSCRIPT

- 1017
1018 Figure 1. Sketch of the Girona River basin. Location of the model area is indicated
1019 through the red polygon beside the coastline.
1020 Figure 2. Geomorphologic sketch of the Girona River alluvial plane.
1021 Figure 3. Location of the rainfall observatories used for event reconstruction and
1022 hydrologic modeling.
1023 Figure 4. Rainfall intensity at Isbert and Gallinera observatories (a), and Guadalest
1024 reservoir (b) during the October 2007 event.
1025 Figure 5. Post-flood surveys information and area used for hydraulic model evaluation.
1026 Figure 6. Pictures taken after the October 2007 event: a) Flood marks at Divina Aurora
1027 street (El Verger); b) House destroyed at the right river bank in El Verger; c) Crevasse
1028 splay deposits at El Verger.
1029 Figure 7. Observed and simulate hydrographs at the Guadalest Reservoir for all the
1030 events used for model calibration and validation.
1031 Figure 8. Simulate hydrographs of the Girona River. The red solid line represents the
1032 simulated hydrograph obtained calibrating the initial soil storage based on post-flood
1033 information. The grey-shaded area lines represents the simulated hydrograph range
1034 obtained using initial soil moisture spanning from 35% to 60% of soil saturation
1035 capacity.
1036 Figure 9. Flooded area and flood depth obtained with the final simulation of the
1037 hydraulic model, under flow conditions of $515 \text{ m}^3 \text{ s}^{-1}$.
1038 Figure 10. Geomorphologic map of the model area.
1039 Figure 11. Cross sections of the Girona River floodplain.
1040 Figure 12. Longitudinal section of the Girona River. Talweg (solid line), right river
1041 bank (dashed line), left river bank (points).
1042 Figure 13. Infrastructures altering flow propagation.
1043 Figure 14. Model simulations and activation thresholds with different flow conditions a)
1044 $360 \text{ m}^3 \text{ s}^{-1}$; b) $515 \text{ m}^3 \text{ s}^{-1}$; c) $900 \text{ m}^3 \text{ s}^{-1}$.
1045
1046
1047
1048
1049 Only for black and white edition:
1050 Figure 1. Sketch of the Girona River basin. Location of the model area is indicated
1051 through the polygon beside the coastline.
1052
1053
1054

1055 We simulated the Girona River flash flood using hydrologic and hydraulic models
1056
1057 Models results were validated with post-flood surveys
1058
1059 The connection between geomorphologic structure and flooded area was analyzed
1060
1061 We identified flood activation thresholds in different geomorphic elements
1062

